

Strong equilibrium in FEA – an alternative paradigm?

Maunder, Edward¹; Ramsay, Angus²

ABSTRACT

This paper presents a brief review of some recent and current research in the formulation and application of hybrid equilibrium elements, with emphasis on the design and assessment of structures. The aim is to highlight the means and the benefits of obtaining fully equilibrated solutions from finite element models. The mechanics of the formation of an element stiffness matrix is presented in physical terms, and this is followed by two areas of application: (i) regarding lower bound (safe) limit analysis of plates with particular attention to the use of the von Mises yield criterion for steel; and (ii) the determination of load paths in a masonry arch. The latter is modelled by faceted thick shell equilibrium elements, and a solid hexahedral equilibrium element is also proposed for modelling the voussoirs. We conclude that there is much scope for equilibrium models to be a valuable tool for structural engineers.

Keywords: finite elements, equilibrium, limit analysis, load paths.

1. INTRODUCTION

Demonstration of equilibrium is a key requirement in the design or assessment of structures, and this requirement is embodied in Codes of Practice throughout the world. However, the precise meaning of the term is somewhat ambiguous in practice. This ambiguity played its part in the collapse of the Sleipner offshore oil platform in 1991 [1].

Finite element methods (FEM) are one of the commonest forms of analysis, but it raises a paradox that, in the authors' opinion, demands a paradigm shift in the use of FEM. The paradox: we seek equilibrium but in practice base FEM analysis on compatibility, i.e. from an assumed set of deformed shapes, FEM determines that combination which best satisfies physical laws, or in mathematical terms minimizes the total potential [2]. Unless we can prove otherwise, the solution is approximate although satisfying compatibility and Hooke's law. The approximation reveals itself by its lack of local equilibrium, and therein lies the paradox.

There is another way of formulating FEM, which is to assume a set of stress fields that equilibrate with the loads, and determine the combination that gets closest to satisfying compatibility. Although this leads to another approximation to the true solution, local and global equilibrium is strictly satisfied and the approximation is revealed by its lack of compatibility. For the safe design of structures we believe, to quote Ed Wilson [3]: "equilibrium is essential, compatibility is optional"

So the question arises: why don't we take more advantage of "strong" equilibrium via assumed stress fields in equilibrium finite elements (EFE), as opposed to "weak" equilibrium as derived from assumed displacement fields in compatible finite elements (CFE)?

¹ College of Engineering, Mathematics & Physical Sciences, University of Exeter (UK). (Corresponding author) e.a.w.maunder@exeter.ac.uk

² Ramsay Maunder Associates (UK) angus_ramsay@ramsay-maunder.co.uk

The seeds of strong equilibrium in EFE were actually sown some 50 years ago [4], but software development for commercial use took the easier path towards CFE. So much investment has been put into CFE that there is now little knowledge of alternatives, and there is resistance to changing the status quo unless industry demands it. However, in general, industry is unaware of strong equilibrium as a possible alternative! It should be noted that equilibrium models also have an important role to play in dual analyses for the purposes of verification and error estimation.

2. AN EQUILIBRIUM FORMULATION

We follow the concept of the hybrid equilibrium element [5], where we assume: (i) internal stress fields σ that satisfy the differential equations of equilibrium

$$\sigma = \mathbf{S}\hat{\mathbf{s}} + \sigma_0 \quad (1)$$

where the columns of \mathbf{S} form a basis of self-equilibrating fields and σ_0 denotes a particular stress field that balances the distributed loads on an element, and (ii) independent displacement fields \mathbf{v} for each side

$$\mathbf{v} = \mathbf{V}\hat{\mathbf{v}} \quad (2)$$

where the columns of \mathbf{V} form a basis of side displacements. In Eq. (1) and (2) $\hat{\mathbf{s}}$ and $\hat{\mathbf{v}}$ vectors collect the internal stress field and side displacement field parameters respectively.

A weak form of compatibility between the internal strains and the side displacements is expressed:

$$\int_{\Omega} \mathbf{S}^T \boldsymbol{\varepsilon} \, d\Omega = \oint_{\partial\Omega} \mathbf{S}^T \mathbf{N} \mathbf{v} \, d\Gamma \quad (3)$$

where side tractions \mathbf{t} that balance the internal stresses are defined by

$$\mathbf{t} = \mathbf{N}^T \sigma \quad (4)$$

A strong form of equilibrium is then completed by the integral equation:

$$\int_{side} \mathbf{V}^T \mathbf{t} \, d\Gamma = \hat{\mathbf{g}}_{side} = \int_{side} \mathbf{V}^T \bar{\mathbf{t}} \, d\Gamma \quad (5)$$

when the applied tractions $\bar{\mathbf{t}}$ are in polynomial form of no higher degree than that of the side displacement polynomial functions.

The usual form of the hybrid equations for an element is then given in Eq. (6), where the submatrices are also defined:

$$\begin{bmatrix} -\mathbf{F} & \mathbf{D}^T \\ \mathbf{D} & \mathbf{0} \end{bmatrix} \begin{Bmatrix} \hat{\mathbf{s}} \\ \hat{\mathbf{v}} \end{Bmatrix} = \begin{Bmatrix} \mathbf{0} \\ \hat{\mathbf{g}} \end{Bmatrix} \quad \text{with } \mathbf{F} = \int_{\Omega} \mathbf{S}^T \mathbf{f} \mathbf{S} \, d\Omega, \quad \mathbf{D} = \oint_{\partial\Omega} \mathbf{V}^T \mathbf{N}^T \mathbf{S} \, d\Gamma \quad (6)$$

In Eq. (6) we have assumed for simplicity that there are no body forces, and hence the particular stress field σ_0 is zero, and the stress/strain relations are defined by $\mathbf{f}\sigma = \boldsymbol{\varepsilon}$. This equation also allows us to define an element stiffness matrix \mathbf{K} which would allow incorporation into commercial types of FE software.

$$\mathbf{K}\hat{\mathbf{v}} = \hat{\mathbf{g}} \quad \text{where } \mathbf{K} = \mathbf{D}\mathbf{F}^{-1}\mathbf{D}^T. \quad (7)$$

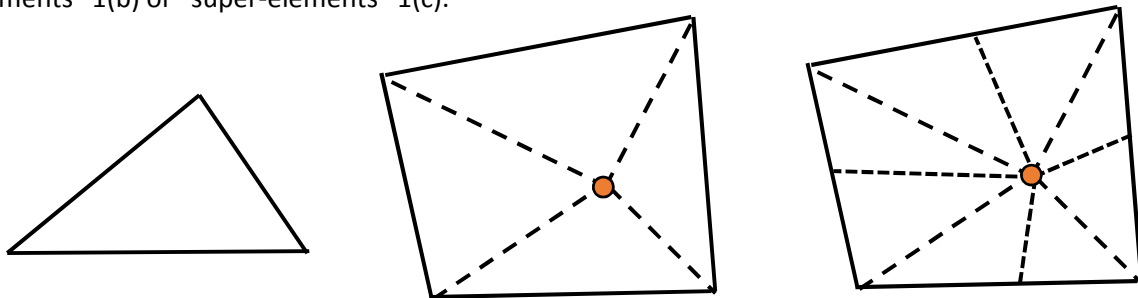
The $\hat{\mathbf{g}}$ vector in Eq. (5) and (6) contains the load parameters which are dual to the displacement parameters.

In a mesh of hybrid equilibrium elements the displacement and traction distributions along a side or face can be associated with an internal structural node, e.g. situated at its centroid, leaving vertex nodes to describe the initial geometry of an element. The usual shape of element to be used as a building block is triangular in 2D and tetrahedral in 3D, and the sides or faces of these elements, termed “primitive” are assumed to be straight or flat respectively. Curved boundaries introduce a degree of complexity in the formulation that is usually not necessary when curves can be well enough represented by a series of small straight segments. Similar formulations have been proposed for hybrid equilibrium elements in the contexts of modelling plates and curved shells [6] when the latter can reasonably be assumed to be in faceted form.

When modelling 2D and 3D continua, stress fields in a mesh are fully equilibrated both internal to the elements and across their interfaces, and it is only required that the normal and tangential shear stresses be codiffusive. Thus the other stress components at an interface may be discontinuous. However, it is usually found in practice that a good level of continuity is obtained unless the mesh is relatively coarse and there are high stress gradients.

However, a single primitive element suffers from a kinematic instability referred to as spurious kinematic modes, otherwise known as pseudo-mechanisms. These are due to the property that certain side displacements do zero work with any of the tractions that equilibrate with the internal stress field approximations, and hence these displacements are unconstrained. A consequence of this is that an element stiffness matrix \mathbf{K} is rank deficient by more than the number of rigid body modes.

Nevertheless, when primitive elements, as in Fig.1(a) are assembled into a mesh such pseudo-mechanisms may be blocked by neighbouring elements. Stable configurations can always be guaranteed by assembling patches of elements, e.g. as illustrated in Fig.1, into so-called “macro-elements” 1(b) or “super-elements” 1(c).



(a) triangular primitive element (b) quadrilateral macro-element (c) quadrilateral super-element

Figure 1. Examples of hybrid equilibrium elements.

A macro-element can have any polygonal form and generally it has as many primitive elements as the number of vertices on its boundary, e.g. the quadrilateral in Fig.1(b) has 4 primitives. Pseudo-mechanisms are generally blocked although some internal ones may exist depending on the position of the internal vertex. These pseudo-mechanisms would not be excited by loads on the sides, or loads distributed internally defined by continuous functions of position.

A super-element subdivides the macro-element with additional nodes on its external sides and retains a single internal node as illustrated in Fig.1(c). Although the additional nodes on the straight sides allow local pseudo-mechanisms to exist, they are not activated by the continuous modes of traction that are

assumed to act on their sides, with their amplitudes collected in vector $\hat{\mathbf{a}}$. The internal stress fields tend to be enriched compared to the simpler macro-element.

For a super-element, we assemble the stiffness matrices of the constitutive primitive elements, as defined in Eq.(7), and then eliminate the internal degrees of freedom so as to form a stiffness matrix \mathbf{K}_s where:

$$\mathbf{K}_s \hat{\mathbf{v}}_s = \hat{\mathbf{g}}_s \quad (8)$$

and vectors $\hat{\mathbf{v}}_s, \hat{\mathbf{g}}_s$ collect displacement and traction parameters of the external sides of the primitive elements. Eq.(8) is consistent when tractions $\hat{\mathbf{g}}_s$ are obtained by projecting the continuous tractions $\hat{\mathbf{a}}$:

$$\hat{\mathbf{g}}_s = \mathbf{A} \hat{\mathbf{a}} \Rightarrow \hat{\mathbf{v}}_s = \mathbf{K}_s^+ \hat{\mathbf{g}}_s \text{ and } \hat{\mathbf{w}} = \mathbf{A}^T \hat{\mathbf{v}}_s = [\mathbf{A}^T \mathbf{K}_s^+ \mathbf{A}] \hat{\mathbf{a}} \quad (9)$$

thus $\hat{\mathbf{w}} = \mathbf{F} \hat{\mathbf{a}}$ where $\mathbf{F} = \mathbf{A}^T \mathbf{K}_s^+ \mathbf{A}$.

In Eq.(9) \mathbf{K}_s^+ denotes the pseudo-inverse of \mathbf{K}_s , and \mathbf{F} denotes the flexibility matrix of the super-element. The selection of continuous traction modes represented by vector $\hat{\mathbf{a}}$ is limited to polynomials of no higher degree than the stress fields, and they may be restricted for convenience of use in design to much lower degrees.

Further research is required in order to evaluate their potential benefits, but we consider that the formulation of a super-element in hexahedral form could be particularly useful in modelling 3D structures as illustrated in Fig.6 of Section 4.

3. LOWER BOUND LIMIT ANALYSIS OF PLATES

Lower bound limit analysis of plates provides a way to maximize economy of material within safe limits. This area is of particular relevance to future emphasis on efficient use of resources with the need to reduce energy use and consequent benefits to climate change [7].

The most commonly used materials are reinforced concrete, for which a square yield criterion for moments is appropriate [8], and steel for which the von Mises yield criterion is most appropriate [9, 10]. When moment actions predominate, transverse shear forces are not accounted for in the yield criteria, and equilibrium in the sense of Kirchhoff plate theory can be used.

The ultimate limit state for ductile plates, such as those being considered here, is plastic collapse and the Eurocodes, EC2 for reinforced concrete and EC3 for structural steel, explicitly allow plastic analysis to be used to calculate the stress resultants at collapse. Limit analysis, which is one form of plastic analysis, has the property that the predicted collapse load is independent of any residual stress field. Also, by dint of the fact that it does not include the strengthening phenomena of membrane action as the plate deforms out of the initial plane, and strain hardening, it provides a conservative prediction of the actual plastic collapse load.

Limit analysis can, of course, be considered in a finite element context and one of the earliest approaches adopted meshes of rigid triangular elements with the boundaries of the elements being potential yield lines, [11]. In the context of the plasticity theorems, this is a kinematic approach leading to an upper bound prediction of the collapse load. The mesh produces a vector space of potential collapse mechanisms and linear programming is used to find the pattern with the lowest collapse load.

The problem with this approach, however, is that the collapse load is extremely sensitive to the geometry of the yield line pattern and unless geometric optimisation of the this pattern is also undertaken then the predicted collapse load can be significantly greater than the true value. This was discussed in [12] where more modern upper bound software (which does undertake geometric optimisation) was compared with the lower bound solutions from EFE for a reinforced concrete landing slab.

Lower bound limit analysis for plates is not commonly practised due to an absence of commercial software to implement such analysis. The software developed by the authors is based on EFE, and it has been verified when using the square yield criterion. This was relatively straightforward since there is a large body of theoretical solutions and benchmark problems available in the literature, [12]. The same is not the case for the elliptical criterion, and so conventional finite element analysis was adopted using an elastic, perfectly-plastic material model to produce reference solutions, see [13] for example.

To demonstrate the influence of the yield criterion on the collapse load we consider a rectangular plate of uniform thickness t . The plate spans a distance a , is simply supported on two opposite sides of length b , and supports a uniformly distributed load (pressure) p . This plate configuration would often be idealised as a simply supported beam by practising engineers but as will be demonstrated, whilst beam theory produces results that are independent of the beam width b , this is not the case for beams when idealised as plates and made from ductile steels which obey the elliptical yield criterion of von Mises.

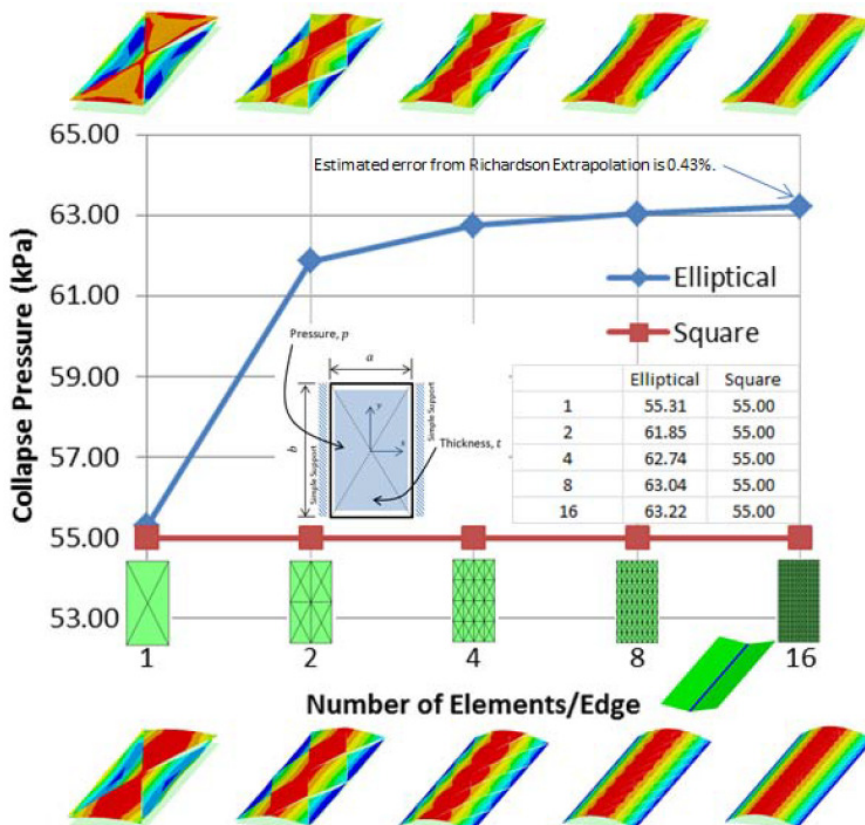


Figure 2 Convergence of the lower bound limit load (pressure) using either the square or the elliptic yield criterion. Note that contour plots of utilization are included for each mesh at the top and bottom of the figure corresponding to the elliptical and the square criterion respectively.

This plate is analysed in a form of lower bound limit analysis using EFE with both types of yield criteria. A sequence of mesh refinements was adopted as shown in Fig.2 for a convergence study, with span $a = 0.6\text{m}$, support width $b = 1.2\text{m}$, thickness $t = 6\text{mm}$, and yield stress = 275MPa . When the square yield criteria is adopted, the collapse mechanism is simply a sagging yield line across the centre of the plate and the theoretical value of the collapse load or plastic limit load is given by Eq.(10):

$$p_c = 2 \left(\frac{t}{a} \right)^2 \text{ yield stress} = 55\text{kPa} \quad (10)$$

The meshes shown in Fig.2 are comprised of regular grids of triangular elements. The boundaries of these elements are composed of their corner nodes or vertices as well as their sides. The actual tractions on a side consist of normal and torsional moments and transverse shear forces. For a hybrid equilibrium element these are represented by the normal moments and equivalent shear forces, which incorporate the effects of torsional moments, together with concentrated transverse forces at the vertices, as indicated in Fig.3.

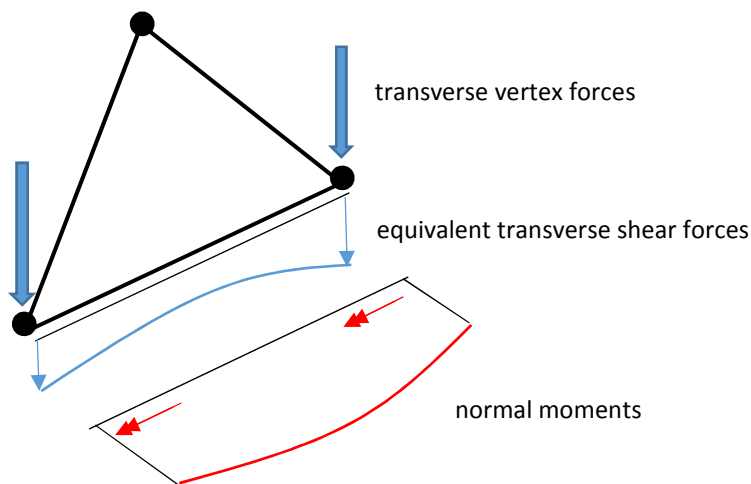


Figure 3. Side tractions and vertex forces for a Kirchhoff hybrid equilibrium plate element.

EFE determines the Cartesian moment fields at collapse and these can be combined into an equivalent moment field appropriate to the yield criterion being adopted, e.g. as defined in Eq(12)

In [14] we presented an implementation relevant to reinforced concrete slabs, based on the square yield criterion of Nielsen. This form of analysis complements the more widely used method of yield line analysis which produces upper bounds to collapse loads for RC slabs – again based on Nielsen.

Our solution is formed by combining hyperstatic fields of stress-resultants in matrix \mathbf{B} with a particular solution \mathbf{m}_0 that equilibrates the applied load, where all static fields are generated within a mesh of equilibrium elements, i.e. as in Eq. (11):

$$\mathbf{m} = \lambda \mathbf{m}_0 + \mathbf{B}\mathbf{X} \quad (11)$$

where λ is the load factor and \mathbf{X} is a vector of parameters that combine the hyperstatic fields. The results in Fig.2 were obtained from piecewise quadratic moments fields \mathbf{m}_0 to balance the uniformly distributed load, and piecewise linear moment fields for the hyperstatic fields.

The maximisation of a load factor then entailed second order cone programming [15]. However when we consider steel (metallic) plates, we find that the Nielsen criterion continues to be used in the context of yield line methods. Whilst this may be easier to understand and implement, it appears to be inappropriate since the von Mises yield criterion is better suited to steel. In this case our method of

solution is readily adaptable to von Mises, and it is summarised in Eq. (12) to (14). Research into this method is ongoing and will be reported in a future publication.

$$\mathbf{m}_{vM} = \sqrt{\mathbf{m}^T \mathbf{P} \mathbf{m}} \leq m_p \quad \text{where} \quad \mathbf{m} = \begin{Bmatrix} m_x \\ m_y \\ m_{xy} \end{Bmatrix}, \quad \mathbf{P} = \frac{1}{2} \begin{bmatrix} 2 & -1 & 0 \\ -1 & 2 & 0 \\ 0 & 0 & 6 \end{bmatrix}. \quad (12)$$

Since \mathbf{P} is symmetric and positive definite, it can be factorized as a product of 2 symmetric and positive definite matrices:

$$\mathbf{P} = \mathbf{Q}^T \mathbf{Q} \quad \text{where} \quad \mathbf{Q} = \frac{1}{\sqrt{2}} \begin{bmatrix} \sqrt{1+0.5\sqrt{3}} & -\sqrt{1-0.5\sqrt{3}} & 0 \\ -\sqrt{1-0.5\sqrt{3}} & \sqrt{1+0.5\sqrt{3}} & 0 \\ 0 & 0 & \sqrt{6} \end{bmatrix} \quad (13)$$

Then $\mathbf{m}_{vM} = \sqrt{\tilde{\mathbf{m}}^T \tilde{\mathbf{m}}}$, when $\tilde{\mathbf{m}} = \mathbf{Q} \mathbf{m}$, and the lower bound optimization problem becomes: maximise λ subject to the inequality constraints imposed by the 4D cones illustrated in Fig.4.

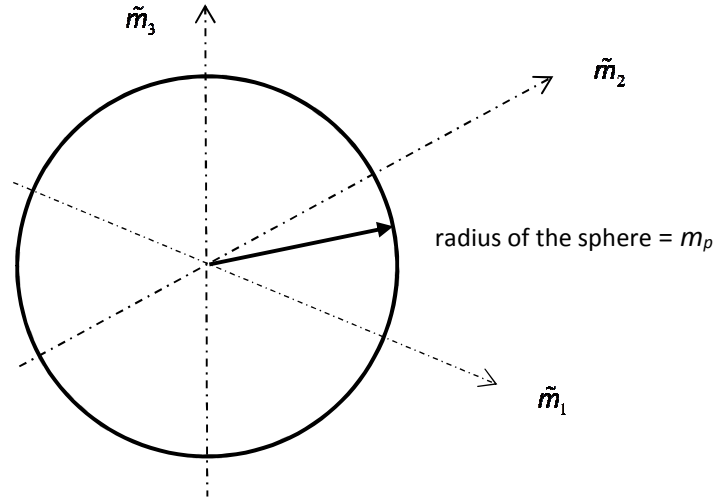


Figure 4. A cross-section of the 4D cone shown as a sphere in 3D.

$$m_{vM} \leq m_p \quad \text{and} \quad \tilde{\mathbf{m}} = \begin{bmatrix} \tilde{\mathbf{m}}_0 & | & \tilde{\mathbf{B}} \end{bmatrix} \begin{Bmatrix} \lambda \\ \mathbf{X} \end{Bmatrix} \quad (14)$$

where $\tilde{\mathbf{m}}_0 = \mathbf{Q} \mathbf{m}_0$, $\tilde{\mathbf{B}} = \mathbf{Q} \mathbf{B}$ and $m_p = \frac{\sigma_p t^2}{4}$ is the plastic bending moment per unit width at a constraint point.

It is noted that only one cone is required per constraint point for a plate, when we assume isotropic homogeneous material with no distinction between yielding in tension or compression. A grid pattern of constraint points is used within each element so as to effectively capture the maximum value of m_{vM} .

The distribution of utilisation in the plate can be shown as a contour plot of the ratio of the equivalent moment field to the yield moment or moment capacity of the plate. The distributions of utilisation are shown in Fig.2 with mesh refinement for the two yield criteria.

It is interesting to note that for the square yield criterion, whilst the plastic limit load is essentially independent of mesh refinement, the distribution of utilisation does change significantly. One should recall, though, that in limit analysis, whilst the collapse load is unique, the moment field at collapse is not, i.e., there are potentially many collapse moment fields with the same collapse load.

When the elliptical yield criterion is adopted then the plastic limit load is no longer independent of the mesh but converges to a value slightly greater than 63kPa as the mesh is refined. This demonstrates that plates of this aspect ratio obeying the elliptical yield criteria can take $63/55 \cong 1.145$ more load than those obeying the square criterion. The reason for this is that the elliptical criteria allows the development of secondary or transverse moments not available when the square criteria is adopted, thereby increasing the load carrying capacity of the plate. The development of these transverse moments is limited by the plate width, b , with long narrow plates being essentially unable to develop any significant transverse moment and, as such, producing collapse loads for the elliptical criteria that are virtually identical to those of the square criterion. This idea is illustrated in Fig.5 which shows the two yield curves and the collapse moments at the critical centre point of the plate for plates at different ends of the range of aspect ratio $= b/a$.

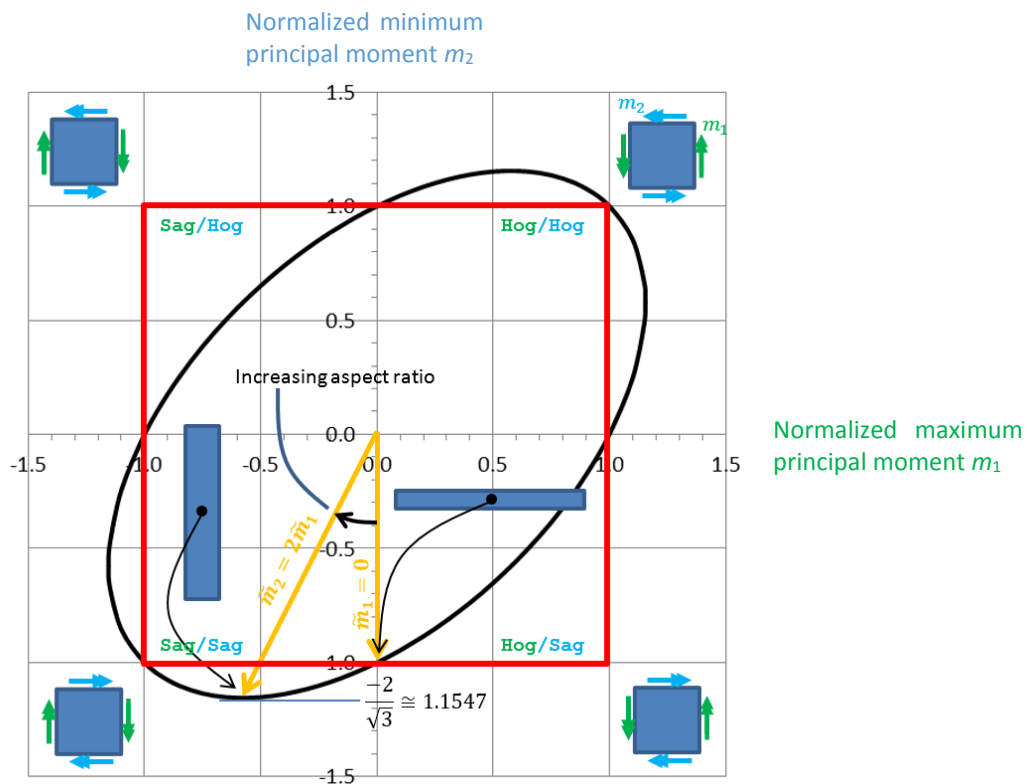


Figure 5 Yield curves and moments at plastic collapse as a function of plate aspect ratio

If the collapse load from the elliptical criteria is normalised (divided by) that from the square criteria then a sigmoid curve is obtained when the normalised collapse load is plotted against plate aspect ratio – see Fig.6.

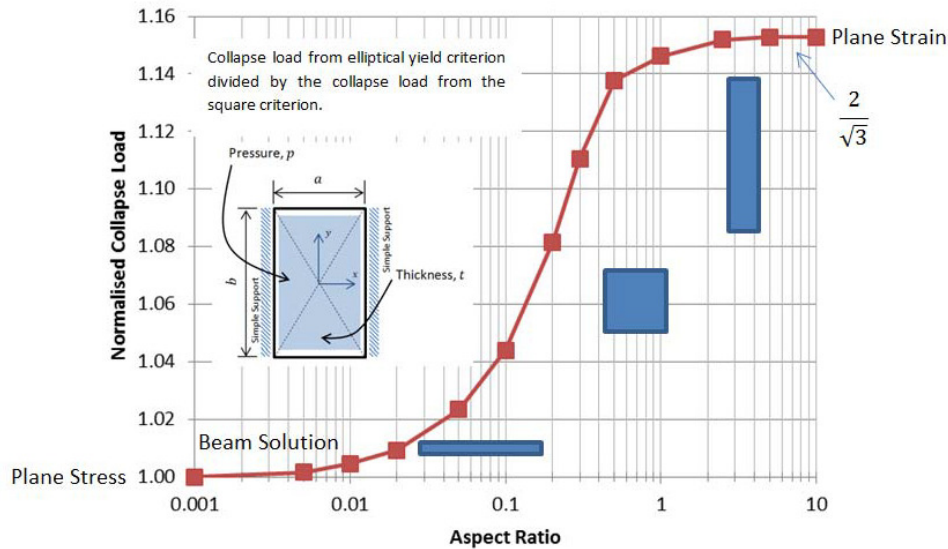


Figure 6 Normalised collapse loads versus aspect ratio.

At the left-hand side of the graph, the curve asymptotes to unity where the collapse load is independent of the chosen yield criterion. At the right-hand side of the graph, the curve asymptotes to $2/\sqrt{3}$ which is approximately 1.155.

This study has shown that significantly different plastic collapse loads may be obtained using the square and elliptical yield criteria. In the case shown, the square yield criterion provides a conservative prediction of the collapse load, and thus the use of the elliptic yield criterion would lead to a more economic design.

4. LOAD PATHS

Design or assessment of structures based on knowledge of an equilibrated set of forces (tractions) to describe possible load paths, i.e. interactions between structural components. Although detailed knowledge of stress fields are not necessarily required, it is essential that these interactions be in equilibrium. Whilst finite element mathematical models are popular in this context, the use of conventional conforming finite element models is problematic.

In such models interactions between elements are represented by generalized forces which include those quantities associated with the nodes positioned at their vertices. Since the vertices are not uniquely associated with an interface, its interactions are not well defined. Alternatively, the interactions may be determined as the resultants of the stresses derived on the faces of the elements. Unfortunately these stresses are not generally codiffusive and they indicate a localized lack of equilibrium! To reduce this lack of equilibrium to an acceptable level may require mesh refinements and associated re-analyses.

Equilibrating tractions can however be recovered by appropriate stages of post-processing [5,16] although, to the authors' knowledge, these are not generally available in commercial software.

The use of hybrid equilibrium elements in finite element models precludes the problems associated with conforming models. A simplified mesh of elements that captures the essential geometry of the structure is sufficient, and its output directly includes the resultant tractions as interactions between element faces. Although mathematical in origin, they have direct physical significance to the engineer.

We illustrate this feature in an example of a masonry arch. There is current concern regarding modelling the behavior of historical arches and viaducts subject to repeated and increasing traffic loads. Local damage can occur under service loads, which could lead to increased risk to life or property, and the usual simplifying assumptions regarding effective strips for 2D structural models used in practice for assessment are considered dubious and inadequate [17].

A simplified finite element model is being developed that serves to carry out sensitivity studies on load paths and behavior when subject to service loads. This model is created generally from an assembly of quadrilateral flat shell elements, with some interface spring elements introduced to represent local damage, e.g. to the mortar joints. An arch which serves to typify is based on a span and width of 10m, a constant radius of 6.25m to the mid-surface, and a consequent rise of 2.5m. The thickness is 0.6m and the masonry is assumed to be linear elastic with Young's modulus = 40kN/mm² and Poisson's ratio = 0.2.

A uniform mesh of flat rectangular macro-elements is used with 10 elements around the arc and 11 elements across the width, as illustrated by the dashed lines in Fig.7, which represents the original undeformed shape. The vertices of the elements lie on the mid-surface, and this arrangement implies that the geometry of the arc is represented by an inscribed polygon having 10 sides.

The load considered is vertically downward and uniformly distributed as 100kN/m² of surface area restricted to the single element as indicated in Fig.8, self-weight is not included in this analysis. The results shown in Figs. 7 and 8, where the deformed shape is shown by the solid lines, correspond to (i) allowing the arch to freely rotate at the abutments and to spread due to a horizontal stiffness of 100kN/mm per element, and (ii) allowing the arch to effectively hinge at the crown (with rotational stiffness of 10,000kNm/radian per element) as the arch spreads.

The hybrid nature of the elements allows side translations and rotations to be included in the results, and these are linked where required by interface joint elements with appropriate stiffnesses. For the case considered the maximum horizontal spread is 0.044mm at each abutment and the maximum vertical deflection at the crown is 0.075mm. These small movements indicate that the arch is sensitive to support conditions and is able to adapt its response by the flexibility of its joints.

Fig.7 illustrates the conventional types of result in the form of contours of circumferential membrane stress-resultants, as well as the deformed view as defined by the displacements of the sides of the hybrid elements. It should be noted that the stress-resultants are fully equilibrated but nevertheless discontinuities can exist in the hybrid equilibrium model as explained in Section 2. Local discontinuities can be observed within the row of elements adjacent to the right abutment of the arch. In part these discontinuities may be explained by the presence of separate spring elements used to represent flexible supports. Such detail in stress is not necessarily required by an engineer interested in explaining how a structure transfers its load. It should also be noted that each such diagram only covers one component of stress resultant. Stress trajectories could also be envisaged, but these would be problematic to obtain in 3D! We believe that the free body diagram approach is readily obtainable and easier to exploit.

Fig.8 presents the resultant membrane force vectors on the sides of the elements which align with (i) the abutment (shown in blue) nearest to the load (shown in green), and (ii) the centre line across the width of the arch (shown in red). These vectors combine the components of normal thrust and horizontal transverse shear force. The vectors belong to a fully equilibrated set of forces belonging to the free body diagram of this part of the arch, and clearly demonstrate how the concentrated load is dispersed across the full width of the arch. Similar 3D diagrams can be formed for other substructures of interest.

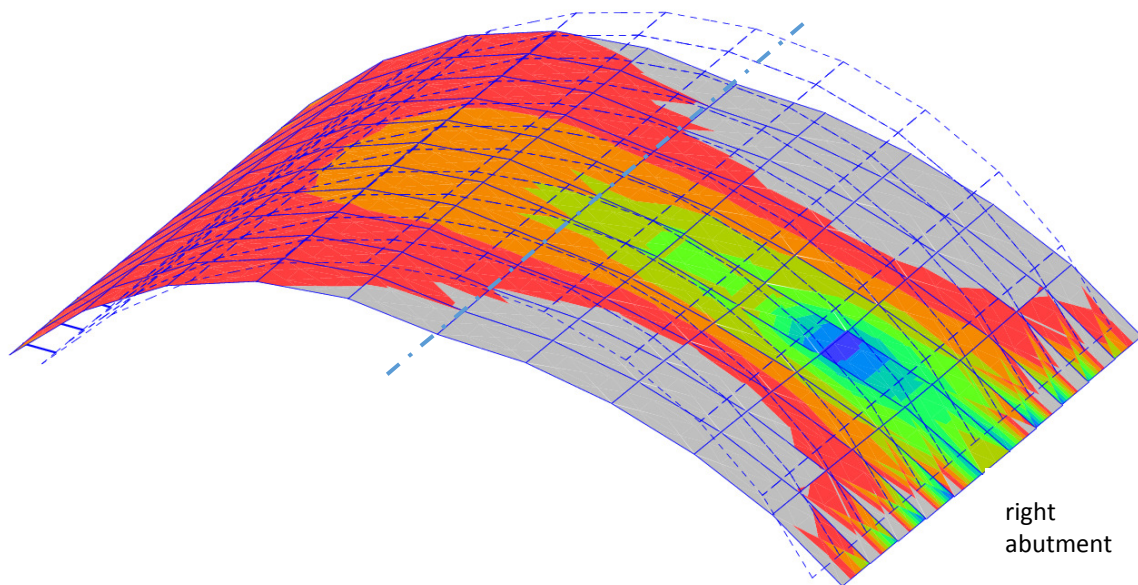


Figure 7. Contour plots of circumferential membrane stress resultants kN/m in compression colour coded from -48.32kN/m (blue) to 0 (red), grey indicates regions in tension.

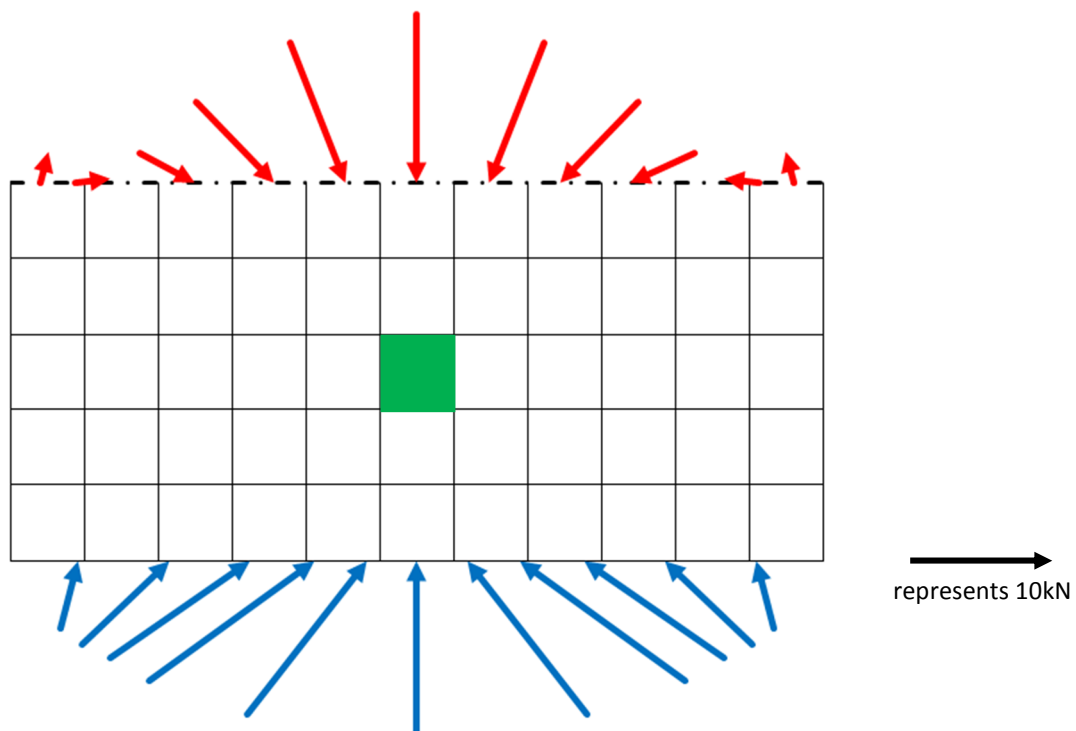


Figure 8. A developed view of half the arch showing a loaded patch and resultant membrane forces acting on the sides of the elements at the crown and the right abutment.

The hybrid equilibrium elements used for the arch model are based on Reissner-Mindlin theory relevant to “thick” plates. However the overall dimensions of the masonry arch imply that a model

based on solid 3D hybrid equilibrium elements could be more relevant. Current research is addressing the development of a hexahedral hybrid equilibrium super-element. Following earlier studies on hexahedral elements reported in [18,19,5], it is proposed to assemble a flat faced hexahedron from 12 tetrahedral “primitive” elements to form a super-element (as discussed in Section 2) as illustrated in Fig.9 to represent a wedge shaped voussoir. The pros and cons of meshing with such hexahedral elements has yet to be fully identified, but it is thought that hexahedral shaped elements could be more appropriate, e.g. for modelling an arch and identifying load paths, compared with tetrahedral shaped elements. For addressing the question of load paths, the assumed traction distributions on the faces of super-elements can be simplified to just the linear ones represented by the 6 stress-resultants of a normal force, two tangential shear forces, two bending moments and a torsional moment.

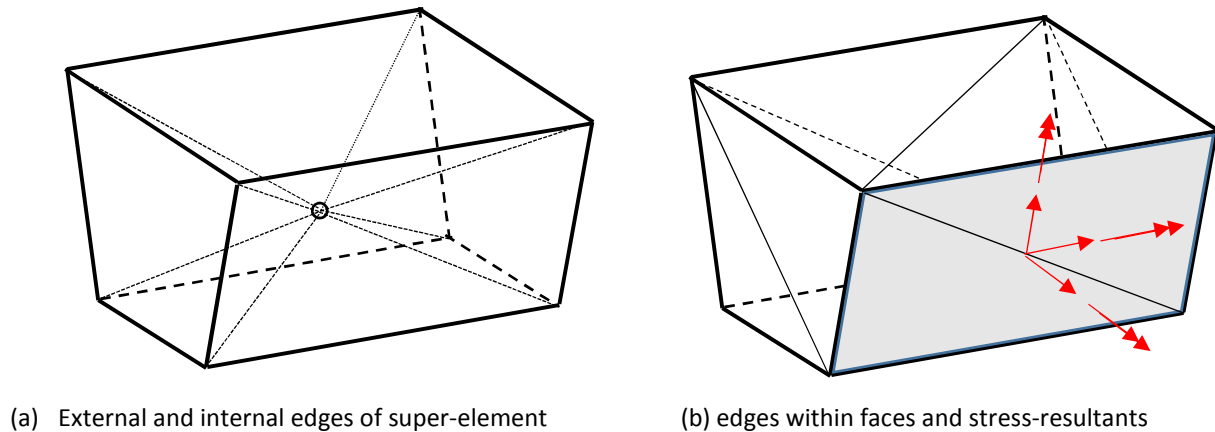


Figure 9. Hexahedral super-element assembled from 12 tetrahedra.

5. CONCLUSIONS

Although the formulation of hybrid equilibrium elements may appear to be more complicated than that of conventional displacement based elements, and they are currently restricted to simpler geometries without curved boundaries, nevertheless they offer distinct advantages to structural engineers. In most situations, equilibrium is of paramount importance although its interpretation is somewhat ambiguous. This ambiguity is absent from equilibrium models which are able to deliver a strong point by point state of equilibrium.

We have demonstrated this ability in the implementation of lower bound limit analysis where a strong form of equilibrium is required in order to guarantee a safe lower bound. Obtaining a strong form of stress equilibrium also implies that stress-resultants over any local surface can be readily determined sure in the knowledge that they are part of a globally equilibrated system.

It is thus concluded that equilibrium finite elements should be an essential part of a structural engineer’s toolkit.

ACKNOWLEDGEMENTS

The authors would like to thank Bill Harvey for his interest in exploiting equilibrium elements in the context of modelling masonry arches, and proposing the typical arch for analysis as discussed in Section 4.

REFERENCES

- [1] Rombach, G.A. (2004). Finite element design of concrete structures. London: Thomas Telford.
- [2] Gallagher, R.H. (1975). Finite Element Analysis Fundamentals. New Jersey: Prentice-Hall.
- [3] Wilson, E.L. (2010). Static & Dynamic Analysis of Structures. Berkeley: Computers & Structures.
- [4] Fraeijs de Veubeke, B.M. (1965). Displacement and equilibrium models in the finite element method. In Stress Analysis (eds. Zienkiewicz O.C. & Holister G.S.). Wiley.
- [5] Almeida, J.P.M., & Maunder, E.A.W. (2017). Equilibrium finite element formulations. Chichester: Wiley.
- [6] Maunder, E.A.W. & Izzuddin, B.A. (2013) A hybrid equilibrium element for folded plate and shell structures. *International Journal for Numerical Methods in Engineering*, 95, 451-477.
- [7] Minimising energy in construction (MEICON), EPSRC Survey Report, 2018
- [8] Nielsen, M.P. & Hoang, L.C. (2011). Limit Analysis and Concrete Plasticity. CRC Press.
- [9] Taylor, G.I. & Quinney, H. (1931). The plastic distortion of metals. *Philosophical Society of London, Series A*, 230, 323-362.
- [10] Canh, L.-V., Hung, N.-X., Hung, N.-D. (2006) Dual Limit Analysis of Plate Bending. In Collection of papers from Prof. Nguyen-Dang Hung's former students (Eds. Géry de Saxcé & Nicolas Moës). Ho Chi Minh City: Vietnam National University.
- [11] Munro, J. & Da Fonseca, A.M.A. (1978). Yield Line Method by Finite elements and Linear Programming. *The Structural Engineer*, 56B, No 2, 37-44.
- [12] Ramsay, A.C.A., Maunder, E.A.W. & Gilbert, M. (2015). Yield Line Analysis of Reinforced Concrete Slabs: Is the 10% Rule Safe? *NAFEMS Benchmark Magazine*, January.
- [13] Ramsay, A.C.A. (2018). Benchmark Challenge Number 2, The NAFEMS Benchmark Challenge – Volume 1, NAFEMS.
- [14] Maunder, E.A.W., & Ramsay, A.C.A. (2012). Equilibrium models for lower bound limit analyses of reinforced concrete slabs. *Computers & Structures*, 108-109, 100-109.
- [15] Alizadeh, F. & Goldfarb, D. (2003) Second-order cone programming. *Math. Prog. Ser B* :95, 3-51.
- [16] Ladevèze, P. & Pelle, J.-P. (2005). Mastering Calculations in Linear and Nonlinear Mechanics. New York: Springer.
- [17] Harvey, W.H. (2019) Second Thoughts on Masonry Bridges. *ASCHB Transactions*, 41, 18-26.
- [18] Pereira, O.J.B. (2008) Hybrid equilibrium hexahedral elements and super-elements. *Communications in Numerical Methods in Engineering*, 24, 157-165.

- [19] Maunder, E.A.W., Moitinho de Almeida, J.P. & Pereira, O.J.B. (2016). The stability of stars of simplicial hybrid equilibrium finite elements for solid mechanics. *International Journal for Numerical Methods in Engineering*, 107, 633-668.